COMMUNICATIONS IN NUMERICAL METHODS IN ENGINEERING
Commun. Numer. Meth. Engng 2001; **17**:495–507 (DOI: 10.1002/cnm.425)

Analysis of singular stresses in bonded bimaterial wedges by computed eigen solutions and hybrid element method

M.-C. Chen[†], K. Y. Sze[*] and Hai-tao Wang

Department of Mechanical Engineering, The University of Hong Kong, Pokfulam Road, Hong Kong SAR, People's Republic of China

SUMMARY

This paper concerns the determination of the singular stress fields in bonded bimaterial wedges under inplane loading. The mathematical complexity required for deriving the eigen solutions is avoided by an *ad hoc* developed one-dimensional finite element formulation. The computed eigen solutions are here adopted in the assumed stress fields of hybrid stress elements which are employed to determine the stress intensities. To illustrate the efficacy of the suggested procedure, stress intensities for cracks in homogeneous, interfacial cracks, bimaterial free edges and other configurations are computed and compared with the existing analytical/reference solutions. Copyright © 2001 John Wiley & Sons, Ltd.

KEY WORDS: bimaterial; stress intensity factor; singularity; hybrid; finite element; crack

1. INTRODUCTION

Co-usage of different materials in modern engineering devices and components has been very common. However, mismatch of the material properties gives rise to singular stresses at the terminating and turning points of the interfaces between dissimilar materials as shown in Figure 1. With the singular stress points taken to co-ordinate origin, the stress fields can be expressed as

$$\sigma_{ij}(r,\theta) = K \cdot r^{\lambda} \bar{\sigma}_{ij}(\theta) \tag{1}$$

where $-1 < \mathrm{Re}(\lambda) < 0$. While the eigenvalue λ characterizes the singularity order, K is the generalized stress intensity factor (SIF) featuring the strength of the singular stress field. Some of the papers on solving λ and $\bar{\sigma}_{ij}$ analytically or numerically have been given in the reference list [1–9]. For problems of finite dimension, numerical methods such as FEM are

[*]Correspondence to: K. Y. Sze, Department of Mechanical Engineering, The University of Hong Kong, Pokfulam Road, Hong Kong SAR, People's Republic of China
[†]On leave from Department of Civil Engineering, East China Jiaotong University, Shuanggang Road, Nanchang 330013, People's Republic of China.

Contract/grant sponsor: Research Grant Council of Hong Kong; contract/grant number: HKU 7083/98E

Received 18 January 2001
Accepted 12 March 2001

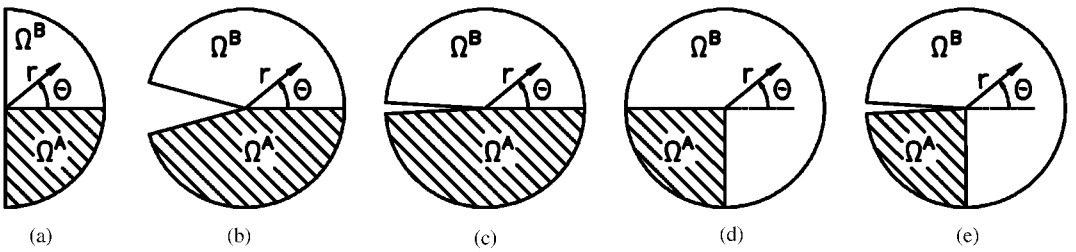

Figure 1. Examples of stress singularities at bimaterial interfaces: (a) free edge; (b) bimaterial wedge; (c) interfacial crack; (d) bonded bimaterial junction; (e) debonded bimaterial junction.

inevitably resorted to for predicting the generalized SIFs. Using the conventional formulation, the accuracy is poor and a large number of elements are required in the vicinity of the singular stress points. In this light, *ad hoc* finite element methods relying on the availability of the eigen solutions have been proposed for enhancing the solution accuracy. Among them, hybrid element methods employ the analytical eigen solutions to formulate the finite element models via multi-field variational principles [10–14]. SIFs can be solved directly as element internal d.o.f.s and high coarse accuracy was reported. The finite element enrichment method makes use of either analytically or numerically determined eigen solutions to enrich the element displacement fields. To ensure the displacement compatibility, a layer of transition elements must be employed between the enriched elements and the conventional elements [15, 16]. It is noted that all the enriched and transition elements are coupled in the global equation and the method cannot be readily incorporated into conventional finite element programmes. Recently, Tan and Meguid employed their numerically solved eigen solutions to formulate element models for bonded dissimilar isotropic wedges [17]. Unlike the hybrid elements in which displacement compatibility is enforced in a weak sense, the eigen displacement solutions and the nodal displacements are related only by nodal collocation in the elements of Tan and Meguid. In case of cracks, SIFs can also be solved indirectly with coarser meshes by path-independent integral techniques, crack closure techniques, alternating methods, etc. (a review can be found in Reference [18]).

The present paper extends the previous works on hybrid crack-tip elements to the analysis of general bonded bimaterial wedges. The eigen solutions are first obtained by the one-dimensional finite element procedure of Sze and Wang [9] and subsequently used to formulate hybrid singular stress elements which are employed to determine the generalized SIFs. The accuracy of the elements is illustrated by examples.

2. HYBRID SINGULAR STRESS FINITE ELEMENT MODEL

In Reference [9], a one-dimensional finite element procedure has been derived to solve the eigen solution of the following asymptotic displacement field in bimaterial systems:

$$\mathbf{u} = \begin{Bmatrix} u_r(r,\theta) \\ u_\theta(r,\theta) \end{Bmatrix} = r^{\lambda+1} \begin{Bmatrix} U_r(\theta) \\ U_\theta(\theta) \end{Bmatrix} = r^{\lambda+1}\mathbf{U}(\theta) \tag{2}$$

which leads to a stress field of the form given in (1). Accurate predictions were obtained for a large variety of bimaterial problems. To make use of the computed eigen solution to facilitate the determination of the generalized SIFs in finite element calculation, the hybrid-stress method is chosen here due to its sound variational basis and high coarse mesh accuracy of the hybrid crack-tip and notch-tip elements [10, 11, 13, 14, 19]. Hybrid singular stress elements can be formulated by the elementwise Hellinger–Reissner functional

$$\Pi^e = \int_{V^e} \left[-\tfrac{1}{2}(\boldsymbol{\sigma}^e)^{\mathrm{T}}(\mathbf{C}^e)^{-1}\boldsymbol{\sigma}^e + (\boldsymbol{\sigma}^e)^{\mathrm{T}}(\boldsymbol{\partial}\tilde{\mathbf{u}}^e) \right] \mathrm{d}v \tag{3}$$

where V^e is the element domain, $\boldsymbol{\sigma}^e$ is the independently assumed element stress, $\boldsymbol{\partial}$ is the strain–displacement operator and $\tilde{\mathbf{u}}^e$ is the displacement compatible with the adjacent elements. It has been assumed that there are no externally applied forces acting on the element. For $\boldsymbol{\sigma}^e$ taken to be the stress computed from eigen solutions $\mathbf{u}_i = r^{\lambda_i+1}\mathbf{U}_i$'s, we have

$$\boldsymbol{\sigma}^e = \mathbf{C}^e\boldsymbol{\partial}(r^{\lambda_1+1}\mathbf{U}_1)\cdot\beta_1^e + \mathbf{C}^e\boldsymbol{\partial}(r^{\lambda_2+1}\mathbf{U}_2)\cdot\beta_2^e + \cdots = \mathbf{C}^e(\boldsymbol{\partial}\mathbb{S}^e)\boldsymbol{\beta}^e \tag{4}$$

where

$$\mathbb{S}^e = [r^{\lambda_1+1}\mathbf{U}_1, r^{\lambda_2+1}\mathbf{U}_2, \ldots] \quad \text{and} \quad \boldsymbol{\beta}^e = \{\beta_1^e, \beta_2^e, \ldots\}^{\mathrm{T}} \quad \text{is the vector of stress coefficients}$$

Let the compatible displacement be expressed symbolically as

$$\tilde{\mathbf{u}}^e = \mathbb{M}\mathbf{q}^e \tag{5}$$

in which $\mathbf{q}^e$ is the element nodal displacement vectors. With the last two equations, (3) becomes

$$\Pi^e = -\tfrac{1}{2}(\boldsymbol{\beta}^e)^{\mathrm{T}}\mathbb{H}^e\boldsymbol{\beta}^e + (\boldsymbol{\beta}^e)^{\mathrm{T}}\mathbb{G}^e\mathbf{q}^e \tag{6}$$

where

$$\mathbb{H}^e = \int_{V^e} [(\boldsymbol{\partial}\mathbb{S}^e)^{\mathrm{T}}\mathbf{C}^e(\boldsymbol{\partial}\mathbb{S}^e)]\,\mathrm{d}v \quad \text{and} \quad \mathbb{G}^e = \int_{V^e} [(\boldsymbol{\partial}\mathbb{S}^e)^{\mathrm{T}}\mathbf{C}^e(\boldsymbol{\partial}\mathbb{M}^e)]\,\mathrm{d}v$$

For converged eigensolutions, stress equilibrium and the traction-free condition over the free wedge faces can be assumed for $\boldsymbol{\sigma}^e$. By virtue of the divergence theorem,

$$\mathbb{H}^e = \int_{S^e} ([\mathbf{n}^e\mathbf{C}^e(\boldsymbol{\partial}\mathbb{S}^e)]^{\mathrm{T}}\mathbb{S}^e)\,\mathrm{d}s \quad \text{and} \quad \mathbb{G}^e = \int_{S^e} ([\mathbf{n}^e\mathbf{C}^e(\boldsymbol{\partial}\mathbb{S}^e)]^{\mathrm{T}}\mathbb{M}^e)\,\mathrm{d}s \tag{7}$$

in which S^e denotes the entire element boundary with the traction-free wedge faces excluded, matrix $\mathbf{n}^e$ contains components of the outward normal to S^e such that $\mathbf{n}^e\boldsymbol{\sigma}^e$ gives the surface traction. The stationary property of Π^e with respect to $\boldsymbol{\beta}^e$ gives

$$\mathbb{H}^e\boldsymbol{\beta}^e = \mathbb{G}^e\mathbf{q}^e \quad \text{or} \quad \boldsymbol{\beta}^e = (\mathbb{H}^e)^{-1}\mathbb{G}^e\mathbf{q}^e \tag{8}$$

and thus

$$\Pi^e = \tfrac{1}{2}(\mathbf{q}^e)^{\mathrm{T}}[(\mathbb{G}^e)^{\mathrm{T}}(\mathbb{H}^e)^{-1}\mathbb{G}^e]\mathbf{q}^e \tag{9}$$

The matrix enclosed within the square brackets is the element stiffness matrix. For the employed assumed stress, the element stiffness matrices for geometrically similar elements are

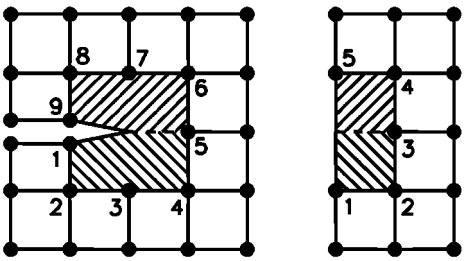

Figure 2. A nine-node notched element and a five-node free-edge bimaterial element interfaced with four-node elements.

identical. The conversion of the domain integrals to boundary integrals is particularly advantageous in the sense that the element displacement $\tilde{\mathbf{u}}^e$ needs only to be defined along the boundary. The displacement interpolation functions of the adjacent elements can be directly employed to secure compatibility. For instance, piecewise linear interpolation is employed in each boundary segment for the nine-node notched and five-node free-edge bimaterial elements depicted in Figure 2.

While real eigen solutions, denoted as $r^{\lambda_i^{\mathrm{R}}+1}\mathbf{U}_i^{\mathrm{R}}(\theta)$ where λ_i^{R} and $\mathbf{U}_i^{\mathrm{R}}$ are both real, can be employed directly in (4), that is not the case for complex eigen solutions. It is trivial to show that if $r^{\lambda_j^{\mathrm{C}}+1}\mathbf{U}_j^{\mathrm{C}}(\theta)$ is an eigen solution, its complex conjugate $r^{\bar{\lambda}_j^{\mathrm{C}}+1}\bar{\mathbf{U}}_j^{\mathrm{C}}(\theta)$ must also be an eigen solution. Without loss of generality, $\mathrm{Im}(\lambda_j^{\mathrm{C}})$ is assumed to be positive. To ensure that the displacement and the stress are real, the two conjugate eigen solutions can be combined as

$$\mathbf{u}_j = \tfrac{1}{2}(\beta_{j\mathrm{R}}^e - \mathrm{i}\beta_{j\mathrm{I}}^e) r^{\lambda_j^{\mathrm{C}}+1}\mathbf{U}_j^{\mathrm{C}} + \tfrac{1}{2}(\beta_{j\mathrm{R}}^e + \mathrm{i}\beta_{j\mathrm{I}}^e) r^{\bar{\lambda}_j^{\mathrm{C}}+1}\bar{\mathbf{U}}_j^{\mathrm{C}} = \beta_{j\mathrm{R}}^e\,\mathrm{Re}(r^{\lambda_j^{\mathrm{C}}+1}\mathbf{U}_j^{\mathrm{C}}) + \beta_{j\mathrm{I}}^e\,\mathrm{Im}(r^{\lambda_j^{\mathrm{C}}+1}\mathbf{U}_j^{\mathrm{C}}) \tag{10}$$

where the stress coefficients β^e's are real. Hence, the induced element stress is

$$\boldsymbol{\sigma}^e = \mathbf{C}^e[\boldsymbol{\partial}\cdot\mathrm{Re}(r^{\lambda_j^{\mathrm{C}}+1}\mathbf{U}_j^{\mathrm{C}})]\,\beta_{j\mathrm{R}}^e + \mathbf{C}^e[\boldsymbol{\partial}\cdot\mathrm{Im}(r^{\lambda_j^{\mathrm{C}}+1}\mathbf{U}_j^{\mathrm{C}})]\beta_{j\mathrm{I}}^e \tag{11}$$

For two-dimensional plane problems with three rigid body modes, $\dim(\boldsymbol{\beta}^e)$ must be larger than $\dim(\mathbf{q}^e)-3$ or the element will exhibit zero energy deformation modes [20]. For the nine- and five-node elements depicted in Figure 2, the minimum $\dim(\boldsymbol{\beta}^e)$ are thus 15 and 7, respectively. Nevertheless, if the adjacent elements do not possess any zero energy deformation modes, the criterion can be disregarded as the global stiffness matrix is still rank sufficient. Let $\dim(\boldsymbol{\beta}^e)$ be $N+2M$ where N is the number of real eigen solutions and $2M$ is the number of complex eigen solutions; the complete stress shape function matrix and the vector of stress coefficients are

$$\begin{aligned}\mathbb{S}^e &= \mathbf{C}^e(\boldsymbol{\partial}\cdot[r^{\lambda_1^{\mathrm{R}}+1}\mathbf{U}_1^{\mathrm{R}},\ldots,r^{\lambda_N^{\mathrm{R}}+1}\mathbf{U}_N^{\mathrm{R}},\mathrm{Re}(r^{\lambda_1^{\mathrm{C}}+1}\mathbf{U}_1^{\mathrm{C}}),\\ &\qquad \mathrm{Im}(r^{\lambda_1^{\mathrm{C}}+1}\mathbf{U}_1^{\mathrm{C}}),\ldots,\mathrm{Re}(r^{\lambda_M^{\mathrm{C}}+1}\mathbf{U}_M^{\mathrm{C}}),\mathrm{Im}(r^{\lambda_M^{\mathrm{C}}+1}\mathbf{U}_M^{\mathrm{C}})])\\ \boldsymbol{\beta}^e &= \{\beta_1^e,\ldots,\beta_N^e,\beta_{1\mathrm{R}}^e,\beta_{1\mathrm{I}}^e,\ldots,\beta_{M\mathrm{R}}^e,\beta_{M\mathrm{I}}^e\}^{\mathrm{T}}\end{aligned} \tag{12}$$

The eigen solutions are chosen such that the real parts of their eigenvalues are smallest and greater than -1. Moreover, the rigid body rotation ($u_r=0$ and $u_\theta=r$) must be excluded or $\mathbb{H}$ will be non-invertible.

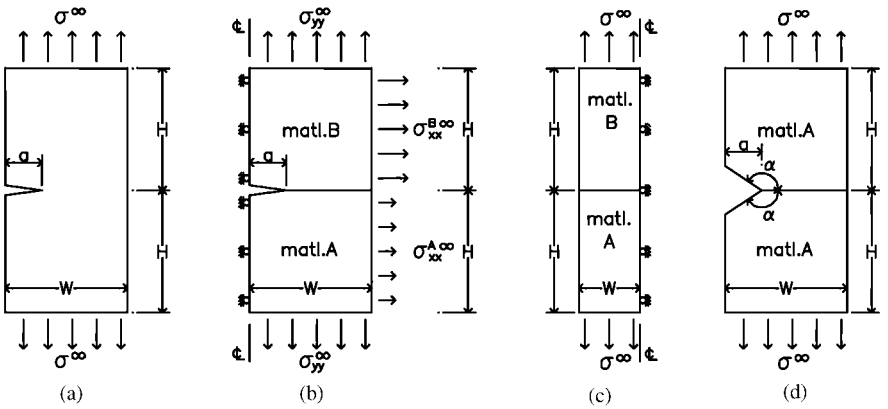

Figure 3. Specimen configurations considered in the numerical examples: (a) single edge crack; (b) central crack; (c) bimaterial free-edge; and (d) bimaterial wedge.

3. NUMERICAL EXAMPLES ON GENERALIZED SIFs

In all examples, Pian–Sumihara [21] four-node hybrid-stress element is employed to interface with the proposed hybrid singular-stress elements. Nine-node notched elements and five-node free-edge elements, see Figure 2, are formulated by using different $\dim(\boldsymbol{\beta}^e)$ which is the number of employed eigen solutions. For the nine- and five-node hybrid singular stress elements, the eigen solutions are obtained by dividing the sectorial domains into eight and four elements in the previous devised finite element procedure [9], respectively, according to the nodal location of the singular stress elements. Furthermore, 10 bubble modes are employed in each sectorial element.

3.1. Single edge cracks

Figure 3(a) shows a single edge plane stress crack in a homogeneous isotropic material under remote traction. The Poisson's ratio is taken to be 0.3. Following Pageau and Biggers [16], the other dimensions are taken to be $H = 2\pi$ and $W = \pi$. Figure 4 shows the three meshes that contain 36, 68 and 122 four-node elements employed to study the problem for a/W equal to 0.3. Table I lists the computed $K_{\mathrm{I}}/(\sigma_{yy}^{\infty}\sqrt{\pi a})$ values for different numbers of eigen solutions employed in formulating the hybrid singular stress element. The ranges of the absolute differences with respect to the infinite strip solution of Keer and Freedman [22] for the results obtained by meshes a–c are 2.084–2.430, 0.798–1.342 and 0.173–0.422 per cent, respectively. The minimum $\dim(\boldsymbol{\beta}^e)$ required to secure the element rank sufficient is 15. The numerical predictions are rather insensitive to the considered range of $\dim(\boldsymbol{\beta}^e)$. Mesh c yields the highest accuracy and is comparable to that obtained by Pageau and Biggers [16] using more than 400 elements in modelling half of the problem domain.

3.2. Interfacial cracks

Figure 3(b) shows half of the rectangular panel that contains a plain stress central crack under biaxial remote traction. Following Lee and Gao [13], the dimensions are taken to be

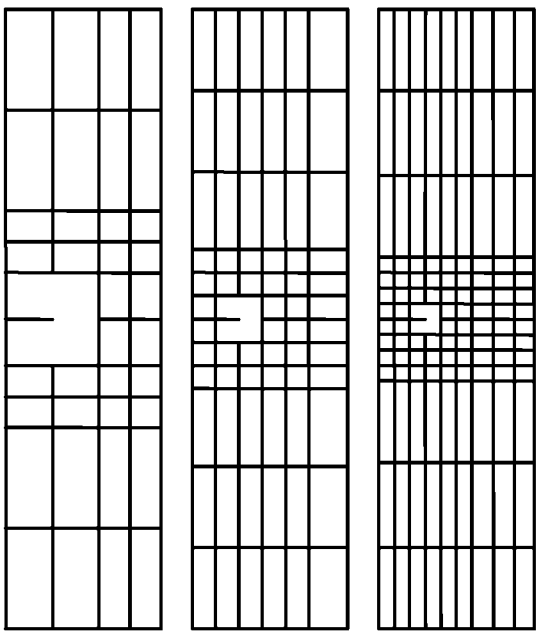

Figure 4. Meshes containing 36, 68 and 122 four-node elements for modelling the single edge crack problem with $a/W = 0.3$ and $H/W = 2$.

Table I. $K_I/(\sigma_{yy}^{\infty}\sqrt{\pi a})$ for single edge crack, reference solution is 1.660 [22].

Mesh	$\dim(\boldsymbol{\beta}^e) = 13$	$\dim(\boldsymbol{\beta}^e) = 15$	$\dim(\boldsymbol{\beta}^e) = 17$	$\dim(\boldsymbol{\beta}^e) = 19$
a	1.61967	1.62228	1.62255	1.62541
b	1.63772	1.63955	1.64151	1.64675
c	1.65300	1.65465	1.65712	1.66308

$H = W = 10a$. The panel is made of two isotropic materials perfectly bonded along the horizontal interface. While both materials have their Poisson ratios set to 0.3, the ratio of their shear modulus μ^B/μ^A is varied. The far-field stresses σ_{yy}^{∞} and $\sigma_{xx}^{B\infty}$ are both taken to be unity. On the other hand, $\sigma_{xx}^{A\infty}$ is determined by requiring the equality of ε_{xx}^A and ε_{xx}^B when the crack is absent. Figure 5 depicts the three meshes with 80, 108 and 404 four-node elements that model half of the panel. They are modified from that of Lee and Gao [13] by employing less elements at regions remote from the crack. In mesh c, there are five columns of element at the left-hand side of the singular stress element. The complex SIFs, K's, defined in [6]

$$\frac{K_I + iK_{II}}{\sqrt{2\pi}} = \lim_{r\to 0} r^{-\lambda}(\sigma_{\theta\theta} + i\sigma_{r\theta})|_{\theta=0} \tag{13}$$

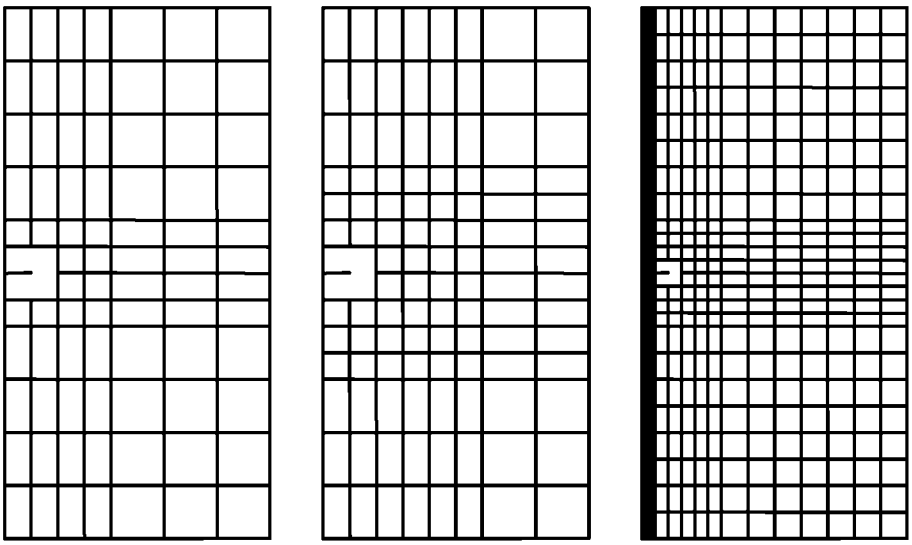

Figure 5. Meshes containing 80, 108 and 404 four-node elements for modelling the central crack problem with $a/W = 10$ and $H/W = 1$.

are computed. In the above equation, λ is the singular eigenvalue. As the crack is small compared to the overall dimensions, the crack-in-infinite-plate solutions can be taken as the reference solutions that are given as [6]

$$K_{\mathrm{I}} + \mathrm{i}K_{\mathrm{II}} = \sigma_{yy}^{\infty}(1 + 2\mathrm{i}|\mathrm{Im}(\lambda)|)(2a)^{\mathrm{i}|\mathrm{Im}(\lambda)|}\sqrt{\pi a} \tag{14}$$

Tables II and III list the computed SIFs by using different meshes and numbers of eigen solutions. The ranges of the absolute differences with respect to the reference solutions by employing meshes a–c for predicting K_{I} are, respectively, 0.365–1.173, 0.288–1.101 and 0.042–0.872 per cent whereas those for predicting non-zero K_{II} are, respectively, 3.536–5.827, 3.546–5.833 and 1.125–3.264 per cent. The minimum dim($\boldsymbol{\beta}^e$) required to secure the element rank sufficient is 15. The numerical predictions are rather insensitive to the considered range of dim($\boldsymbol{\beta}^e$). Moreover, the present errors are consistent with that reported by Lee and Gao [13].

3.3. Bimaterial free-edge

Figure 3(c) shows half of the plane strain rectangular panel formed by two dissimilar isotropic materials subjected to remote traction. Moreover, $H/W = 2$. While both materials have their Poisson ratios set to 0.3, the ratio of their shear modulus μ^B/μ^A is varied. The same problem has been studied by Munz and Yang [23] using standard finite elements. Three meshes containing 28, 46 and 118 four-node elements are employed as shown in Figure 6 to model half of the rectangular panel. Table IV lists exact and computed singular eigenvalues as well as

Table II. $K_I/(\sigma_{yy}^{\infty}\sqrt{\pi a})$ for interfacial cracks.

μ^B/μ^A	Mesh	$\dim(\boldsymbol{\beta}^e)=13$	$\dim(\boldsymbol{\beta}^e)=15$	$\dim(\boldsymbol{\beta}^e)=17$	$\dim(\boldsymbol{\beta}^e)=19$	Reference [6]
	a	0.99378	0.99513	0.99435	0.99635	
1	b	0.99457	0.99591	0.99512	0.99712	1.00000
	c	0.99958	1.00132	1.00306	1.00782	
	a	0.99681	0.99615	0.99572	0.99788	
5	b	0.99757	0.99691	0.99828	0.99864	1.00656
	c	1.00510	1.00480	1.00532	1.00512	
	a	0.99971	0.99915	1.00100	1.00117	
10	b	1.00045	0.99990	1.00175	1.00192	1.01007
	c	1.00861	1.00831	1.00911	1.00891	
	a	1.00313	1.00299	1.00519	1.00524	
100	b	1.00386	1.00372	1.00592	1.00597	1.01483
	c	1.01279	1.01262	1.01376	1.01377	
	a	1.00359	1.00351	1.00567	1.00569	
1000	b	1.00431	1.00424	1.00640	1.00642	1.01542
	c	1.01337	1.01322	1.01432	1.01433	

Table III. $K_{II}/(\sigma_{yy}^{\infty}\sqrt{\pi a})$ for interfacial cracks.

μ^B/μ^A	Mesh	$\dim(\boldsymbol{\beta}^e)=13$	$\dim(\boldsymbol{\beta}^e)=15$	$\dim(\boldsymbol{\beta}^e)=17$	$\dim(\boldsymbol{\beta}^e)=19$	Reference [6]
	a	0.00029	0.00013	0.00021	0.00026	
1	b	0.00029	0.00013	0.0002	0.00026	0.00000
	c	0.0002	0.00005	0.00015	0.00015	
	a	0.10272	0.10219	0.10263	0.10293	
5	b	0.10273	0.1022	0.10264	0.10295	0.09870
	c	0.10021	0.10017	0.09995	0.09981	
	a	0.12752	0.12719	0.12803	0.12817	
10	b	0.12753	0.1272	0.12805	0.12819	0.12220
	c	0.1247	0.12473	0.12478	0.1246	
	a	0.15529	0.15536	0.15655	0.15662	
100	b	0.1553	0.15536	0.15655	0.15663	0.14812
	c	0.15212	0.15225	0.15272	0.15278	
	a	0.15843	0.15858	0.15976	0.15982	
1000	b	0.15843	0.15858	0.15976	0.15983	0.15102
	c	0.15522	0.15541	0.15586	0.15595	

the computed and the reference mode I SIFs which are defined as

$$K_I = \lim_{r\to 0}\left(\frac{r}{W}\right)^{-\lambda}\sigma_{\theta\theta}|_{\theta=0} \tag{15}$$

The exact eigenvalues and the reference SIFs are calculated, respectively, from a scalar and an empirical equation presented by Munz and Yang [23].

The absolute differences of the computed K_I's with respect to their reference solutions by employing meshes a–c are respectively 0.005–1.503, 0.065–1.343 and 0.035–1.406 per cent.

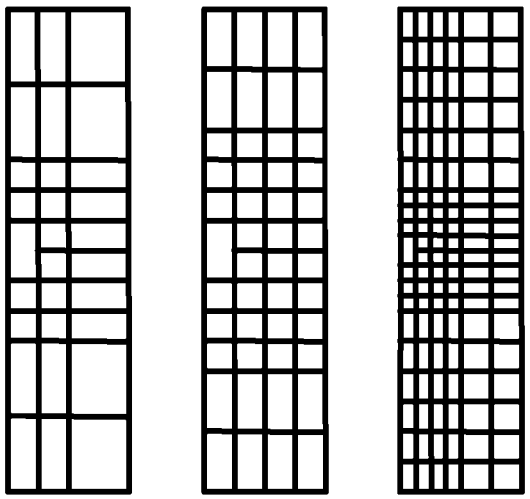

Figure 6. Meshes containing 28, 46 and 118 four-node elements for modelling the bimaterial free-edge problems with $H/W = 2$.

Table IV. Eigenvalues and normalized SIFs $K_1 a^{\lambda}/\sigma_{yy}^{\infty}$ for bimaterial free-edges.

μ^B/μ^A	Computed λ [9] / Exact λ [23]	Mesh	$\dim(\boldsymbol{\beta}^e) = 5$	$\dim(\boldsymbol{\beta}^e) = 7$	$\dim(\boldsymbol{\beta}^e) = 9$	$\dim(\boldsymbol{\beta}^e) = 11$	Reference SIF [23]
5	$\frac{-0.13618}{-0.13618}$	a	0.87951	0.87966	0.878125	0.87584	0.87817
		b	0.87874	0.87885	0.87734	0.87503	
		c	0.87749	0.87954	0.87786	0.87598	
10	$\frac{-0.19846}{-0.19847}$	a	0.84819	0.84748	0.84658	0.84469	0.84067
		b	0.84718	0.84642	0.84552	0.84359	
		c	0.84570	0.84707	0.84612	0.84525	
100	$\frac{-0.27803}{-0.27803}$	a	0.81712	0.81515	0.81508	0.81497	0.80502
		b	0.81583	0.81381	0.81374	0.81356	
		c	0.81438	0.81462	0.81455	0.81634	
1000	$\frac{-0.28772}{-0.28773}$	a	0.81373	0.81163	0.81162	0.81181	0.80204
		b	0.81026	0.81026	0.81025	0.81037	
		c	0.81099	0.81112	0.81111	0.81330	

The minimum $\dim(\boldsymbol{\beta}^e)$ required to secure the element rank sufficient is 7. The numerical predictions are rather insensitive to the considered range of $\dim(\boldsymbol{\beta}^e)$. Pageau and Biggers [16] have also considered the case of $\mu^B/\mu^A = 10$. Their computation using their most refined mesh that contains over 800 elements yields $\lambda = -0.198305$ and $K_1 = 0.7991\sigma^{\infty}/a^{\lambda}$ which

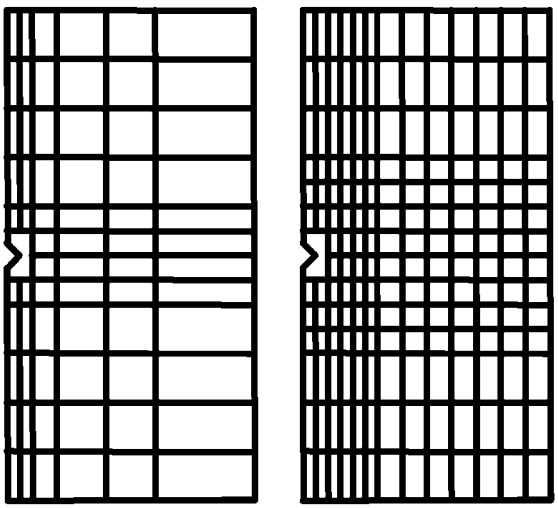

Figure 7. Meshes containing 78 and 178 four-node elements for modelling the bimaterial wedge problem with $a/W = 20$ and $H/W = 1$.

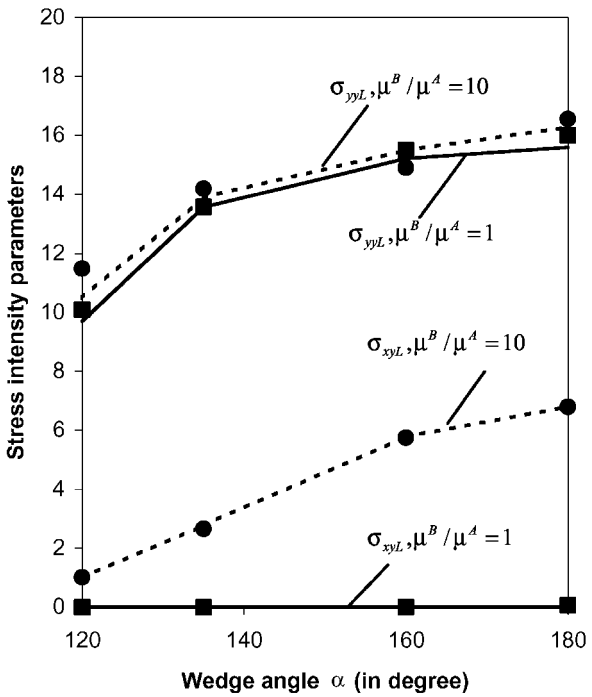

Figure 8. Effect of notch angle on stress intensity parameters. (■) and (●) denote the present predictions for $\mu^B/\mu^A = 1$ and 10, respectively; (—) and (- - -) are the results of Tan and Meguid [17].

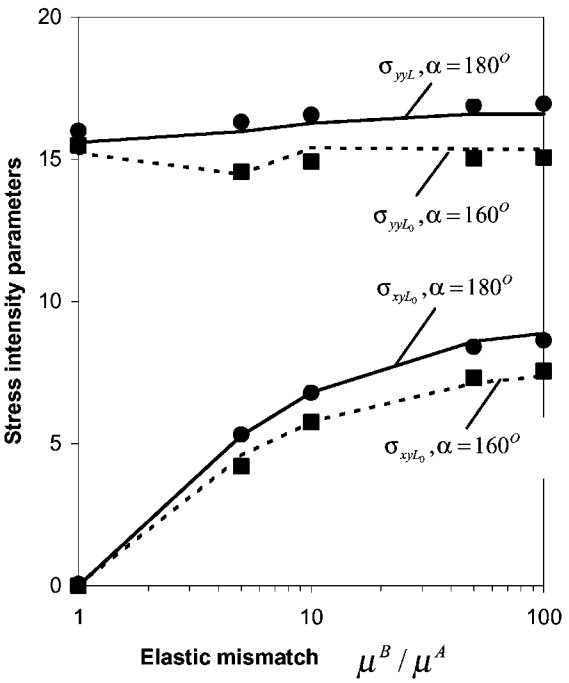

Figure 9. Effect of elastic mismatch on stress intensity parameters. (■) and (●) denote the present predictions for $\alpha = 160$ and 180°, respectively; (—) and (- - -) are the results of Tan and Meguid [17].

are considerably different from the analytic λ ($= -0.19847$) and the reference solution of K_{I} ($= 0.84671\sigma^{\infty}/a^{\lambda}$) as compared to the present predictions.

3.4. *Bimaterial wedges*

Figure 3(d) shows a notched rectangular panel formed by two isotropic material wedges with subtended angle α. Other dimensions include $H = 20a$ and $W = 20a$. As the singular stresses are characterized by not only the stress singularities but also the intensity factors. In other words, it may not be sensible to compare the stress fields in different bimaterial wedges simply by looking at their stress intensity factors. In view of this, Tan and Meguid [17] adopted the following stress intensity parameters σ_{yyL} and σ_{xyL} such that

$$\sigma_{yyL} + \mathrm{i}\sigma_{xyL} = \frac{1}{L}\int_0^L (\sigma_{yy} + \mathrm{i}\sigma_{xy})|_{\theta=0}\,\mathrm{d}r \quad \text{where } L = a/100 \tag{16}$$

to quantify the singular stress fields. Two meshes that contain 78 and 178 four-node elements as shown in Figure 7 are employed for the present study. The range of the difference for σ_{yyL}'s predicted by meshes a and b is 0.071–0.799 per cent whereas that for non-zero σ_{xyL}'s is 0.137–0.203 per cent. In other words, both meshes produce practically identical results. Figures 8 and 9 compare the predictions yielded by mesh b with that of Tan and Meguid [17] for different wedge angles and elastic mismatches. The latter predictions are obtained by

a sectorial singular stress element with radius $a/20$ and 35 nodes along the circumferential direction. It can be seen that the differences between the two sets of predictions are small.

4. CLOSURE

Numerically determined eigen solutions [9] for bimaterial systems are employed to formulate nine-node notched and five-node free-edge hybrid singular stress finite element models. These models can be co-used with any robust four-node plane elements to determine the stress intensities. After studying problems on cracks in homogeneous materials, interfacial cracks, bimaterial free-edges and others, the proposed elements are found to possess high coarse mesh accuracy, insensitivity to mesh density and the number of eigen solutions.

ACKNOWLEDGEMENTS

The work described here was substantially supported by a grant from the *Research Grant Council of Hong Kong* (Project No. HKU 7083/98E).

REFERENCES

1. Williams ML. The stresses around a fault or crack in dissimilar media. *Bulletin of the Seismological Society of America* 1959; **49**:199–204.
2. Pageau SS, Gadi KS, Biggers SB, Joseph PF. Standardized complex and logarithmic eigensolutions for *n*-material wedges and junctions. *International Journal of Fracture* 1996; **77**:51–76.
3. Bogy DB. Two edge-bonded elastic wedges of different materials and wedge angles under surface traction. *Journal of Applied Mechanics* 1971; **38**:377–386.
4. Hein VL, Erdogan F. Stresses singularities in a two-material wedge. *International Journal of Fracture Mechanics* 1971; **7**:317–330.
5. Ting TCT, Chou SC. Edge singularities in anisotropic composites. *International Journal of Solids and Structures* 1981; **17**:1057–1068.
6. Rice JR. Elastic fracture mechanics concepts for interfacial cracks. *Journal of Applied Mechanics* 1988; **55**: 98–103.
7. Chen DH, Nisitani H. Singular stress field near the corner of jointed dissimilar materials. *Journal of Applied Mechanics* 1993; **60**:607–613.
8. Chen HP. Stress singularities in anisotropic multi-material wedges and junctions. *International Journal of Solids and Structures* 1998; **35**:1057–1073.
9. Sze KY, Wang H-T. A simple finite element formulation for computing stress singularities at bimaterial interfaces. *Finite Elements in Analysis and Design* 2000; **35**:97–118.
10. Pian THH, Tong P, Luk CH. Elastic crack analysis by a finite element method. *Proceedings of the 3rd Conference on Matrix Methods in Structural Mechanics*, Wright-Patterson Air Force Base, AFFDL-TR-71-160, 1971; 661–682.
11. Atluri SN, Kobayashi AS, Nakagaki M. An assumed displacement hybrid finite element method for fracture mechanics. *International Journal of Fracture* 1975; **11**:257–271.
12. Chow WT, Beom HG, Atluri SN. Calculation of stress intensity factors for an interfacial crack using dissimilar anisotropic media using a hybrid element method and the mutual integral. *Computational Mechanics* 1995; **15**:546–557.
13. Lee J, Gao H-J. A hybrid finite element analysis of interface cracks. *International Journal for Numerical Methods in Engineering* 1995; **38**:2465–2482.
14. Freitas JA, Ji Z-Y. Hybrid-Trefftz equilibrium model for crack problems. *International Journal for Numerical Methods in Engineering* 1996; **39**:569–584.
15. Benzley SE. Representation of singularities in the isoparametric finite elements. *International Journal for Numerical Methods in Engineering* 1974; **8**:537–545.
16. Pageau SS, Biggers SB. Enrichment of finite elements with numerical solutions for singular stress fields. *International Journal for Numerical Methods in Engineering* 1997; **40**:2693–2713.

17. Tan MA, Meguid SA. Analysis of bimaterial edges using a new singular finite element. *International Journal of Fracture* 1997; **88**:373–391.
18. Atluri SN. *Structural Integrity and Durability*. Tech Science Press: Georgia, 1997.
19. Tong P, Pian THH, Lasry SJ. A hybrid element approach to crack problems in plane elasticity. *International Journal for Numerical Methods in Engineering* 1973; **7**:297–308.
20. Xue W-M, Karlovitz LZ, Atluri SN. On the existence and stability conditions for mixed-hybrid finite element solutions based on Reissners Variational Principle. *International Journal of Solids and Structures* 1985; **21**: 97–116.
21. Pian THH, Sumihara K. Rational approach for assumed stress finite elements. *International Journal for Numerical Methods in Engineering* 1984; **20**:1685–1695.
22. Keer LM, Freedman JM. Tensile strip with edge cracks. *International Journal of Engineering Science* 1973; **11**:1265–1275.
23. Munz D, Yang YY. Stress singularities at interface in bonded dissimilar materials under mechanical and thermal loading. *Journal of Applied Mechanics* 1992; **59**:857–861.

